Dissertation

submitted to the
Combined Faculties for the Natural Sciences and for Mathematics
of the Ruperto-Carola University of Heidelberg, Germany
for the degree of

Doctor of Natural Sciences

Put forward by

Christian Möhler, M.Sc.
Born in Heidelberg, Germany

Oral examination: January 24, 2018

Stopping-power prediction with dual-energy computed tomography

Referees: Prof. Dr. João Seco
Prof. Dr. Oliver Jäkel

Stopping-power prediction with dual-energy computed tomography

A substantial component of range uncertainty in ion therapy is attributed to the prediction of ion stopping-power ratio (SPR) from x-ray computed tomography (CT). Besides imaging technology that uses the same particles as are employed for treatment (e.g., proton CT), dual-energy CT (DECT) has been proposed to potentially improve this prediction within the framework of clinical x-ray CT. The aim of this thesis was to demonstrate improved SPR prediction with DECT from theoretical, experimental and clinical viewpoints.

In the first step, an optimized approach was developed on the basis of a rigorous theoretical framework. Since variability in the SPR of human tissue is dominated by electron density, its universal and accurate determination solves the larger part of the problem and reduces the empirical component to the stopping number, which represents the second factor in SPR. By inferring the stopping number from DECT-derived photon cross sections, linear mixing behavior was demonstrated, which enabled proper calibration and the possibility to quantify uncertainty. The optimized approach was experimentally verified and benchmarked against the clinical gold standard in homogeneous animal tissues (human-like composition) and an anthropomorphic head phantom (human-like geometry). Furthermore, significant range differences to the standard approach were observed in patients, highlighting clinical relevance.

From a methodological and experimental perspective, the developed method of SPR prediction with DECT outperforms the clinical gold standard and reduces the associated uncertainty to below 1 %, which might eventually lead to the reduction of treatment margins.

The thesis is presented in cumulative format and comprises eight peer-reviewed publications.

Reichweitenvorhersage mit der Zwei-Spektren-Computertomographie

In der Ionentherapie ist ein wesentlicher Anteil der Reichweiteunsicherheit auf die Vorhersage des Ionenbremsvermögens (SPR) mittels Röntgen-Computertomographie (CT) zurückzuführen. Anstatt die Bildgebung mit den gleichen Partikeln wie bei der Therapie durchzuführen (z.B. Protonen-CT), wurde die Zwei-Spektren-Computertomographie (DECT) als vielversprechend angesehen, die Vorhersagegenauigkeit der klinischen CT-Bildgebung mit Röntgenstrahlen zu verbessern. Im Rahmen dieser Arbeit wurde diese Hypothese durch theoretische, experimentelle und klinische Untersuchungen überprüft.
Dazu wurde zunächst ein optimiertes Verfahren zur SPR-Vorhersage mithilfe von DECT entwickelt, welches auf einer fundierten theoretischen Basis beruht. Da das Bremsvermögen von menschlichen Geweben maßgeblich von der Elektronendichte abhängt, trägt dessen universale und genaue Bestimmung bereits zur überwiegenden Problemlösung bei und beschränkt den Effekt der Empirie auf die zweite Einflussgröße des Bremsvermögens, die Bremszahl. Leitet man die Bremszahl aus Wechselwirkungsquerschnitten von Photonen her, stellt sich ein lineares Mischungsverhalten ein, welches eine ordnungsgemäße Kalibrierung und Unsicherheitsabschätzung ermöglicht. Diese optimierte Vorgehensweise wurde in homogenen tierischen Geweben (mit menschenähnlicher Zusammensetzung) und in einem anthropomorphen Kopfphantom (mit menschenähnlicher Geometrie) experimentell verifiziert und mit dem derzeitigen klinischen Standardverfahren verglichen. Des Weiteren wurden zwischen beiden Methoden signifikante Reichweiteunterschiede in Patienten festgestellt, die dessen klinische Relevanz betonen.
Im Vergleich zum derzeitigen klinischen Standardverfahren konnte die eigens entwickelte DECT-basierte SPR-Vorhersage aus methodischer und experimenteller Sicht überzeugen und die Unsicherheiten auf unter 1 % verringern, welches schließlich zu einer Verkleinerung von Sicherheitssäumen in der Patientenbehandlung führen kann.
Die vorliegende Doktorarbeit wurde kumulativ angefertigt und umfasst acht von Experten begutachtete Veröffentlichungen.

Contents

List of publications

Peer-reviewed journal articles

4 published, 2 in press, 2 under review

[Ia] Möhler C, Wohlfahrt P, Richter C, Greilich S. Methodological accuracy of image-based electron density assessment using dual-energy computed tomography. *Medical Physics.* 2017;44(6)2429. doi:10.1002/mp.12265

[Ib] Möhler C, Wohlfahrt P, Richter C, Greilich S. Range prediction for tissue mixtures based on dual-energy CT. *Physics in Medicine and Biology.* 2016;61(11)N268. doi:10.1088/0031-9155/61/11/N268

[Ic] Möhler C, Wohlfahrt P, Richter C, Greilich S. On the common foundation of dual-energy CT methods for the determination of electron density and effective atomic number. *Physics and Imaging in Radiation Oncology.* 2017; under review.

[IIa] Möhler C, Russ T, Wohlfahrt P, Elter A, Runz A, Richter C, Greilich S. Experimental verification of particle-range prediction in biological tissue by single- and dual-energy computed tomography. *Physics in Medicine and Biology.* 2017; under review. arXiv:1708.07368

[IIb] Wohlfahrt P[#], Möhler C[#], Richter C[**], Greilich S[**]. Evaluation of stopping-power prediction by dual- and single-energy computed tomography in an anthropomorphic ground-truth phantom. *International Journal of Radiation Oncology*Biology*Physics.* 2017; in press. doi:10.1016/j.ijrobp.2017.09.025
([#]both authors share first authorship, [**]both authors share last authorship)

[IIc] Wohlfahrt P, Möhler C, Greilich S, Richter C. Comment on: Dosimetric comparison of stopping-power calibration with dual-energy CT and single-energy CT in proton therapy treatment planning [Med. Phys. 43(6), 2845-2854 (2016)]. *Medical Physics.* 2017;44(10)5533. doi:10.1002/mp.12418

[IIIa] Wohlfahrt P, Möhler C, Hietschold V, Menkel S, Greilich S, Krause M, Baumann M, Enghardt W, Richter C. Clinical implementation of dual-energy CT for proton treatment planning on pseudo-monoenergetic CT scans. *International Journal of Radiation Oncology*Biology*Physics.* 2017;97(2)427. doi:10.1016/j.ijrobp.2016.10.022

[IIIb] Wohlfahrt P, Möhler C, Stützer K, Greilich S, Richter C. Dual-energy CT based proton range prediction in head and pelvic tumor patients. *Radiotherapy and Oncology.* 2017; in press. doi:10.1016/j.radonc.2017.09.042

Conference contributions

2017

Möhler C, Wohlfahrt P, Richter C, Greilich S. **Talk:** Dual-energy CT for photon therapy — benefits and limitations. Dreiländertagung der Medizinischen Physik, Dresden, Germany, 2017

Wohlfahrt P, Möhler C, Greilich S, Richter C. **Talk:** Dual-energy CT for particle therapy — benefits and limitations. Dreiländertagung der Medizinischen Physik, Dresden, Germany, 2017

Greilich S, Dal Bello R, Jäkel O, Möhler C. **Talk:** Experimental validation of an in-silico model for ion-beam modulation in lung parenchyma. Dreiländertagung der Medizinischen Physik, Dresden, Germany, 2017

Russ T, Runz A, Greilich S, Möhler C. **Poster:** Measurement of tissue stopping-power ratios for ion-range prediction. Dreiländertagung der Medizinischen Physik, Dresden, Germany, 2017

Möhler C, Wohlfahrt P, Richter C, Greilich S. **Talk:** What is needed to demonstrate the benefit of dual-energy CT for particle treatment planning? 56th Annual Conference of the Particle Therapy Co-Operative Group, Yokohama, Japan, 2017

Möhler C, Wohlfahrt P, Richter C, Greilich S. **E-Poster:** Electron-density assessment using dual-energy CT: accuracy and robustness. ESTRO 36, Vienna, Austria, 2017

Wohlfahrt P, Möhler C, Enghardt W, Greilich S, Richter C. **Talk:** Dual-energy CT-based proton treatment planning to assess patient-specific range uncertainties. ESTRO 36, Vienna, Austria, 2017

Dal Bello R, Möhler C, Jäkel O, Greilich S. **E-Poster:** Bragg peak degradation in lung tissue: a compact and complete model. ESTRO 36, Vienna, Austria, 2017

2016

Möhler C, Russ T, Elter A, Latz B, Wohlfahrt P, Richter C, Greilich S. **Talk:** Verbesserung der Reichweitevorhersage in der Ionentherapie durch dichteunabhängige Messung von Röntgen-/ Ionenschwächung tierischer Gewebe. 47. Jahrestagung der Deutschen Gesellschaft für Medizinische Physik, Würzburg, Germany, 2016

Wohlfahrt P, Möhler C, Negwer F, Troost EGC, Enghardt W, Greilich S, Richter C. **Talk:** Dual-energy CT-based assessment of patient tissue variability and its influence on particle therapy planning. 47. Jahrestagung der Deutschen Gesellschaft für Medizinische Physik, Würzburg, Germany, 2016

Möhler C, Wohlfahrt P, Richter C, Greilich S. **Poster:** Robust range prediction for arbitrary tissue mixtures based on dual-energy CT. 55th Annual Conference of the Particle Therapy Co-Operative Group, Prague, Czech Republic, 2016

Wohlfahrt P, Möhler C, Baumann M, Enghardt W, Krause M, Greilich S, Richter C. **Poster:** Clinical implementation of dual-energy CT for proton treatment planning to reduce CT-based range uncertainties. 55th Annual Conference of the Particle Therapy Co-Operative Group, Prague, Czech Republic, 2016

Dal Bello R, Möhler C, Jäkel O, Greilich S. **Talk:** Impact of density heterogeneities on the degradation of clinical C-12 Bragg peaks. 55th Annual Conference of the Particle Therapy Co-Operative Group, Prague, Czech Republic, 2016

Möhler C, Wohlfahrt P, Richter C, Jäkel O, Greilich S. **E-Poster:** Dual-energy CT for range prediction in proton and ion therapy. ESTRO 35, Turin, Italy, 2016

Wohlfahrt P, Möhler C, Jakobi A, Baumann M, Enghardt W, Krause M, Greilich S, Richter C. **Talk:** Clinical use of dual-energy CT for proton treatment planning to reduce CT-based range uncertainties. ESTRO 35, Turin, Italy, 2016

2015

Möhler C, Hünemohr N, Wohlfahrt P, Richter C, Jäkel O, Greilich S. **Talk:** Korrekturfaktoren für die Elektronendichte-basierte Reichweitenvorhersage in der Protonen- und Ionenstrahltherapie. 46. Jahrestagung der Deutschen Gesellschaft für Medizinische Physik, Marburg, Germany, 2015

Wohlfahrt P, Menkel S, Hietschold V, Möhler C, Greilich S, Baumann M, Enghardt W, Krause M, Richter C. **Talk:** Clinical implementation of dual-energy computed tomography (DECT) for treatment planning on pseudo-monoenergetic CT scans (MonoCT) in the proton therapy facility Dresden. 46. Jahrestagung der Deutschen Gesellschaft für Medizinische Physik, Marburg, Germany, 2015

Polster L, Möhler C, Hünemohr N, Wohlfahrt P, Richter C, Jäkel O, Greilich S. **Poster:** Messung von Inhomogenitätseffekten in der Dual-Energy-Computertomographie (DECT) für die Schwerionentherapie-Planung. 46. Jahrestagung der Deutschen Gesellschaft für Medizinische Physik, Marburg, Germany, 2015

List of acronyms

CT	computed tomography
DE	dual energy
DECT	dual-energy computed tomography
DKFZ	German Cancer Research Center
DNA	deoxyribonucleic acid
HIT	Heidelberg Ion Beam Therapy Center
HLUT	Hounsfield look-up table
HU	Hounsfield units
ICRP	International Commission on Radiological Protection
ICRU	International Commission on Radiation Units and Measurements
LINAC	linear accelerator
NCRO	National Center for Radiation Research in Oncology
NIST	National Institute of Standards and Technology
SECT	single-energy computed tomography
SPR	stopping-power ratio
TPS	treatment planning system

Chapter 1

Introduction

1.1 — Motivation

The purpose of radiation therapy is to eliminate or inactivate cancer cells by inducing DNA damage with ionizing radiation. While many types and sources of radiation are conceivable for this purpose, the majority of treatments are nowadays performed with a spectrum of x-ray radiation produced from MeV electrons in a medical linear accelerator (LINAC). With modern techniques of application, various beams of modulated intensity are directed to the target region from different angles to conform dose to the tumor [1]. Sparing the surrounding healthy tissue is thereby only possible to a certain extent due to the physical nature of x-ray dose deposition in tissue, which is maximal a few millimeters below the skin and then decreases with depth (figure 1).

For heavy charged particles, the characteristics of dose deposition are fundamentally different. Ions with therapeutic kinetic energy in the order of 100 MeV per nucleon slow down via electronic collisions, densely ionizing the medium along their path until they finally stop after a certain range. Most of the energy is thereby transferred at the end of their path, forming the so-called Bragg peak. With low dose deposition entering the tissue and a sudden increase at the end of range, the depth-dose curve of ions is 'inverted' compared to the photon profile (figure 1). This potentially allows for better concentration of dose to the tumor and more effective sparing of healthy tissue, in particular behind the target. Therefore, protons and heavier ions have been suggested early on as promising particle candidates for radiation therapy [2].

However, due to the steep gradient at the distal fall-off of the Bragg peak, the delivered dose distribution is susceptible to uncertainty in treatment planning and delivery [5, 6]. Important sources of uncertainty are

- pre-treatment patient imaging, the role of which is (a) to locate anatomical structures such as the target and organs-at-risk; and (b) to serve as a quantitative basis for dose calculation (clinical gold standard: computed

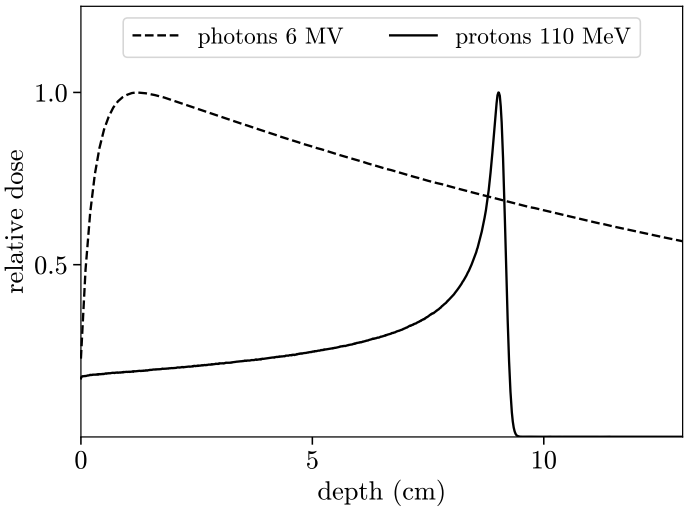

Figure 1: Normalized depth-dose curves of 6 MV photons and 110 MeV protons in water from radiation transport simulations with the FLUKA Monte Carlo code [3, 4].

tomography (CT) — see section 2.3),

- day-to-day variations in patient setup, beam delivery or patient anatomy (e.g., filling of cavities),
- changes in anatomy on a longer time scale (e.g., tumor shrinkage, patient weight loss),
- and organ motion during irradiation.

Different techniques are currently being used or developed for the mitigation of range uncertainty, such as motion management [7, 8], robust optimization [9, 10], or image-guided radiotherapy [11, 12] The remaining uncertainty is accounted for in clinical routine by adding safety margins to the delineated target volume to make sure the tumor is fully covered in any reasonably probable scenario [13]. Typical range margins are composed of an absolute component of 1-3 mm and a relative component of 2.5-3.5 % (figure 2), leading to a considerably increased irradiation of healthy tissue.

Furthermore, range uncertainty is challenging to quantify (as reflected in the variety of margin recipes), so that compromises in beam configuration are often being made for safety reasons. For example, it is avoided to direct a beam frontally at an organ-at-risk [6]. Since this usually leads to a suboptimal dose distribution, the quantification and ideally reduction of range uncertainty is essential to profit from the dosimetric advantage of ion therapy.

From figure 2, it is evident that the treatment of a tumor that is not seated in the first few centimeters below the skin would profit particularly from a reduction of

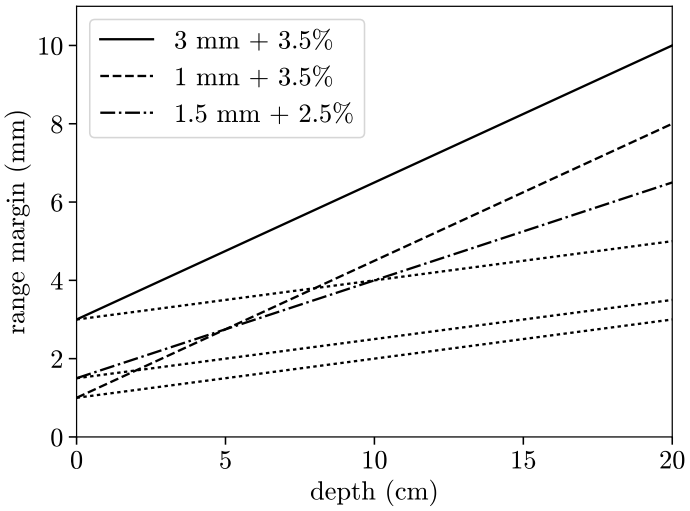

Figure 2: Typical range margin recipes used in different proton therapy centers: MD Anderson Proton Therapy Center, Houston and Loma Linda University Medical Center (3 mm + 3.5 %); MGH Proton Beam Therapy Center, Boston (1 mm + 3.5 %); and UF Health Proton Therapy Institute, Jacksonville (1.5 mm + 2.5 %) [5]. Dotted lines indicate how the respective margins would change if the relative uncertainty component was limited to 1 %.

the relative component of range uncertainty (i.e., the slope). This component is dominated by the prediction of ion stopping-power ratio (SPR) on the basis of the planning CT image (section 2.3). Due to conversion between the interaction mechanisms of different particle types (x-ray photons for imaging and ions for treatment), this prediction is affected by substantial uncertainty of about 1-3 % [5, 14–17].

The conversion problem promises to be solved if the same particles were used for both imaging and treatment. This would naturally be the case for proton or heavier ion CT [18,19]. However, the according technology is still in development phase [20] and it is not clear whether a clinical system with suitable characteristics will be available any time soon.

Nevertheless, advancement in SPR prediction might already be possible within the framework of clinical x-ray CT. In 2006, the first commercial dual-energy computed tomography (DECT) scanner was launched to market [21]. Scanning the patient with two separated x-ray energy spectra grants access to the underlying radiological tissue parameters, such as electron density and photon cross section or effective atomic number [22–24]. These parameters have been used for SPR prediction with DECT [25–27]. Thereby, the impact of the empirical component of SPR prediction is strongly mitigated, which in return should reduce the associated CT-related component of range uncertainty in ion therapy.

1.2 — AIM OF THIS THESIS

Many methods are available today to determine material properties such as electron density or effective atomic number from DECT data [22–24, 26–34]. Either, they were already published shortly after the invention of computed tomography, or they were triggered by the clinical introduction of DECT in recent years. Before the start of this dissertation project, it was not clear, which of the many published methods would be best suited and how to optimally exploit the determined tissue parameters for SPR prediction.

Furthermore, experimental results on the hypothesized superiority of DECT-based SPR prediction methods had been inconclusive, especially with regard to their transferability to complex human morphology and tissue composition. This is partly owing to the fact that methods for direct verification of ion stopping power or range in patients are currently not accurate enough to serve as a reliable reference. Finally, it also remained unclear how a potential advantage would translate into clinical application.

Therefore, the aim of this thesis was to clarify whether SPR prediction can be improved using clinical DECT, thus potentially limiting CT-related range uncertainty to 1 % (figure 2). The steps taken towards achieving this aim were

- **methodological development** of a rigorous mathematical and physical framework for the prediction of SPR with DECT and the translation of its results into the implementation of an optimized approach,
- **experimental verification** of the refined approach using established validated references and its benchmark against the clinical gold standard,
- and finally assessment of its **clinical relevance**.

After description of the background (chapter 2), an overview of the main results of the publications included in this thesis is presented (chapter 3) and the original manuscripts are provided (chapter 4), followed by a comprehensive discussion (chapter 5) and summary (chapter 6).

Chapter 2

Background

2.1 — Stopping power of ions in matter

The stopping power of ions in matter is defined as the mean energy loss per unit path length, $S = -dE/dx$. The stopping power due to electronic collisions is given by the Bethe formula [35]

$$S = k_0 \, n \frac{z^2}{\beta^2} L(\beta) \,, \tag{2.1}$$

where n is the electron density of the medium, z and β are the charge and relativistic velocity of the projectile, L is the so-called stopping number and k_0 is composed of natural constants taking the value

$$k_0 = 4\pi(\hbar c \alpha)^2/(m_\mathrm{e} c^2) = 5.1 \times 10^{-25} \ \mathrm{MeVcm}^2 \,. \tag{2.2}$$

In the energy regime relevant to ion therapy, it is admissible to write the stopping number in an approximated form (figure 3, appendix A1),

$$L \approx L(\beta, I) \approx \ln\left(\frac{2 m_\mathrm{e} c^2 \beta^2}{1-\beta^2}\right) - \beta^2 - \ln I \,, \tag{2.3}$$

where the only remaining dependencies are the velocity, β, and the mean excitation energy or 'I-value', I (appendix A2).

It is a useful convention in radiotherapy treatment planning to normalize a quantity, x, to its respective value for water, x_w, to obtain a dimensionless quantity $\hat{x}$. From this point on, we usually refer to quantities such as electron density or stopping number in this way. The suffix 'relative to water' is hereby mostly omitted to increase readability, as it can be easily inferred from context. An exception to this guideline is the stopping power relative to water, which will be referred to in this thesis by convention as the stopping-power ratio (SPR).

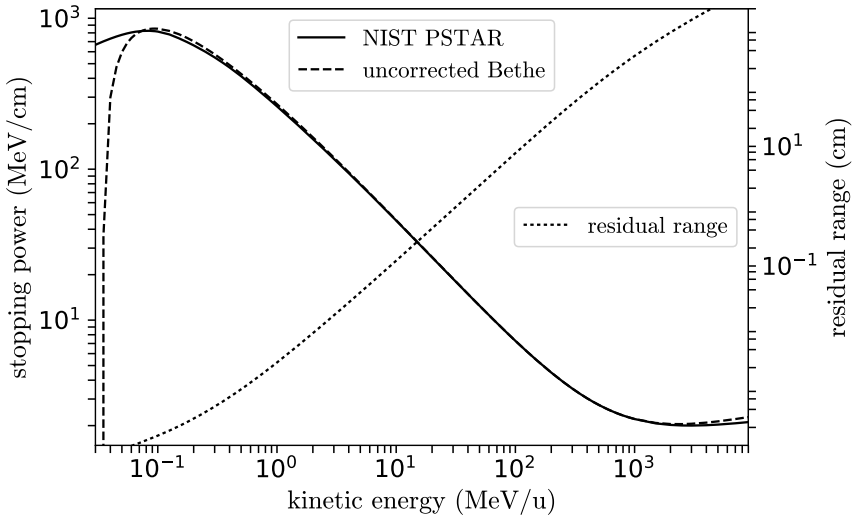

Figure 3: Stopping power and residual range of protons in water. The stopping power was obtained from the PSTAR database of the National Institute of Standards and Technology (NIST) [36] (solid line) and from an independent calculation using the uncorrected Bethe formula (equations 2.1 and 2.3, dashed line). The deviations at high (low) energy are mainly due to the density (shell) effect, well out of the energy window relevant to ion therapy (appendix A1).

Taking this ratio in the Bethe formula 2.1, all prefactors, and in particular the dependency on z^2/β^2, cancel out and SPR reduces to a simple product of electron density and stopping number (cf., section 2.1.2 in pub. Ib), that is

$$\widehat{S} = \widehat{n}\widehat{L}\,. \tag{2.4}$$

With the approximation of equation 2.3, the relative stopping number,

$$\widehat{L} = \frac{L(\beta, I)}{L(\beta, I_\mathrm{w})} = \frac{\ln \frac{2m_\mathrm{e}c^2\beta^2}{1-\beta^2} - \beta^2 - \ln I}{\ln \frac{2m_\mathrm{e}c^2\beta^2}{1-\beta^2} - \beta^2 - \ln I_\mathrm{w}} \tag{2.5}$$

shows only a minor dependence on β, and thus the kinetic beam energy [Ib, figure 1]. Consequently, even the last projectile-related dependence in equation 2.4 is practically removed. In this respect, SPR can be viewed as a pure material quantity, depending only on electron density and stopping number or I-value of the material traversed.

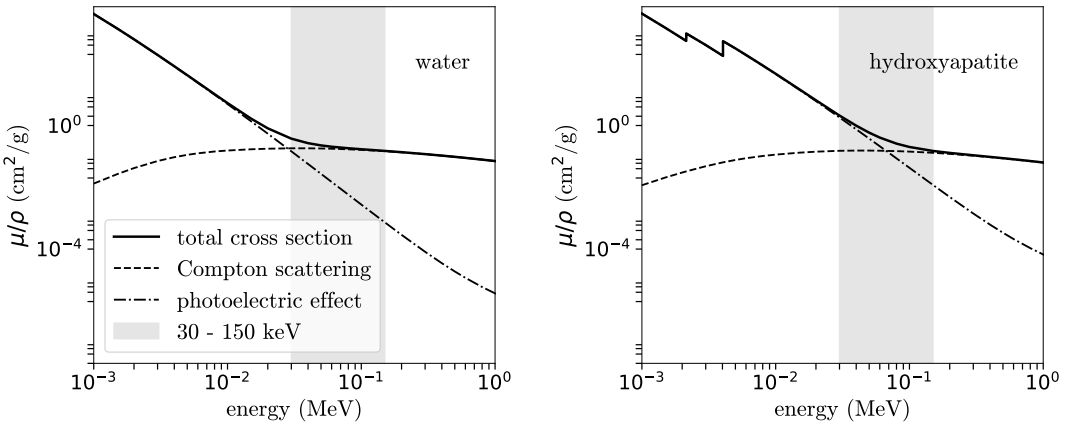

Figure 4: Energy dependence of the mass attenuation coefficient (μ/ρ) of photons in water (left) and hydroxyapatite (right). In contrast to Compton scattering, the photoelectric effect features a strong dependence on energy (x-axis) and material composition (difference between water and hydroxyapatite). Data taken from NIST XCOM Photon Cross Section Database [38].

2.2 — Photon absorption and (dual-energy) computed tomography

The photon attenuation coefficient, μ, depends on electron density and electronic cross section (cf., section 2.A in pub. Ia and section 2.1.1 in pub. Ib) such that

$$\widehat{\mu} = \widehat{n}\widehat{\sigma}\,. \tag{2.6}$$

The cross section is usually expressed as a sum of different interaction mechanisms [37] (cf., appendix A in pub. Ia). In the relevant energy regime of x-ray photons used in medical imaging (30-150 keV), photon attenuation is dominated by the photoelectric effect and (incoherent) Compton scattering (figure 4). The Compton cross section is nearly flat in energy between 30 and 150 keV and more importantly, virtually independent of material composition. The photoelectric cross section, on the other hand, shows a strong dependence on both photon energy, E, and atomic number of the attenuating material, Z, and is roughly proportional to Z^3/E^3.

Computed tomography (CT) displays the spatial distribution of photon attenuation coefficients in the imaged object. For convenience, these are linearly transformed to obtain the CT number in Hounsfield units (HU),

$$\xi = (\widehat{\mu} - 1) \cdot 1000\,\mathrm{HU}\,. \tag{2.7}$$

In the original publication presenting computed tomography [39], Hounsfield al-

ready suggested the use of two different tube voltages to distinguish materials of high atomic number. Shortly after, specific algorithms for material decomposition in terms of a photoelectric and Compton component [22, 40, 41], or electron density and effective atomic number [23,24] were suggested. However, it was not until 30 years later that the first dedicated DECT scanner was brought to market [21]. The introduced 'dual-source' system contains two pairs of an x-ray tube and corresponding detector mounted at an angle of approximately 90 degrees. The CT scanner is therefore capable of an increased scanning speed, which is particularly useful for time-resolved cardiac imaging [21, 42, 43]. The possibility of operating the two tubes at different voltages thus allowing for spectral applications came as an additional feature. Meanwhile several technical implementations of clinical DECT exist [44, 45].

2.3 — State-of-the-art stopping-power prediction

2.3.1 Basic principle

The current state-of-the-art imaging modality for treatment planning is x-ray computed tomography due to its high geometrical fidelity (for delineation and treatment planning) and the dependence of the CT number on electron density (for dose calculation). In order to use the CT image for the latter purpose in ion therapy, it has to be transformed to a 3D map of SPR. CT number and SPR show a strong overall correlation for human tissue due to

i the mutual linear dependence on electron density;

ii correlation between some of the involved radiological parameters (e.g., electron density and atomic number);

iii correlation in elemental composition (humans mainly consist of water, lipid and protein).

Therefore, a fully heuristic one-to-one calibration curve for the voxelwise conversion of CT number to SPR is a practicable solution.

2.3.2 Calibration

Usually a calibration curve is implemented and calibrated in clinical practice as a piece-wise linear function, often referred to as Hounsfield look-up table (HLUT). Two basic recipes are widespread for the calibration procedure of a HLUT, namely the 'empirical' [46] and the 'stoichiometric' [47] method.

In both methods, a set of tissue surrogates is scanned employing the same CT acquisition and reconstruction parameters that are used for treatment planning.

In the 'empirical' method, pairs of CT number and reference SPR (calculated or measured) are then directly interpolated or fitted to obtain a calibration curve. The stoichiometric method contains an intermediate step to account for the fact that tissue surrogates might not be exactly tissue equivalent. Here, the tissue surrogates are first used to fit a CT number model, which then allows for the calculation of 'virtual' CT numbers of tabulated human tissues [48].

The reader is kindly referred to figure 2 in publication IIa and figure 2 in publication IIIa for two examples of a calibrated HLUT.

2.3.3 Limitations

The CT-number-to-SPR conversion is inherently ambiguous, since different physical interaction mechanisms are connected: x-ray photons for imaging; ions for treatment. Its empirical nature thus implicates certain limitations of the HLUT approach:

- The calibration is **not unique**: two materials can have the same CT number, but different SPR and vice versa.
- The definition of a specific calibration curve contains an **element of arbitrariness**. Their is no consensus about how many line segments should be used or whether water should be included as calibration material.
- An HLUT is static and **not patient-specific**, ignoring natural variability in tissue composition within one patient or between patients of, for example, different sex, age or pathology [48].
- Implants and other **non-tissue materials** are generally **not represented** by a HLUT and can hence generate errors in the dose distribution [IIIa, figure 2].

Chapter 3

Overview of results

The major results of the publications included in this thesis are summarized, structured according to the three steps defined in section 1.2. The original manuscripts are provided in chapter 4.

3.1 — Methodological development (Ia-c)

A major aim of this thesis was to develop an optimized approach for accurate SPR prediction with DECT on the basis of a rigorous physical and mathematical framework.

The baseline of the established approach is the reduced version of the Bethe formula as a simple product of electron density and stopping number (equation 2.4). The variability in SPR is dominated by the variability in electron density since the stopping number is contained in an interval of about 0.96 for bone to 1.02 for adipose [Ib, section 2.2]. In publication Ia, we demonstrated that the intrinsic methodological uncertainty for electron-density determination via a simple one-parametric linear-blending formula is below 0.2%, independently of the spectral combination or DECT technology. Furthermore, we proposed a simple way of calibration and quantified its uncertainty.

In addition, it was realized that the evaluated formula is mathematically equivalent to the corresponding one derived by Brooks [24]. This equivalence is in fact not immediately evident. The same holds true for Brooks' derivation of the effective atomic number. The mathematical equivalence of the algorithms described in references [24,26,28,30,31,34] was therefore demonstrated in a second publication [Ic]. Furthermore, while a coherent definition of the effective atomic number was already included in appendix A.2 of publication Ia, the strong interlink between electron density and effective atomic number determination is highlighted in clarity in publication Ic.

The determination of the second factor entering SPR prediction, that is, the stopping number or equivalently the I-value, is less straightforward as it has no direct

analogue in photon absorption and thus requires an empirical proxy. Methods relying on the effective atomic number, as often used in previous publications on the topic [25–27], lack a coherent treatment of tissue mixtures, which is an essential feature in patient CT images due to finite voxel size. In publication Ib, we demonstrated how a convenient linear mixing behavior arises when using the photon attenuation cross section instead of the effective atomic number as a proxy. The publication includes a detailed mathematical derivation as well as a discussion of conceptual and practical advantages of the proposed approach.

3.2 — Experimental verification (IIa-c)

Extensive experimental verification of the developed DECT method was performed in two complementary environments, each focusing on one of the two relevant aspects of complexity influencing SPR prediction accuracy in a patient: tissue composition (in publication IIa) and geometric morphology (in publication IIb).

Since there is still a remaining, yet small, empirical influence in DECT-based SPR prediction in form of the stopping-number look-up table [Ib], experimental verification in biological tissue is crucial. For this, a hybrid experimental setup and workflow for combined DECT and ion-range mesurement based on a dedicated 3D-printed sample container was developed and continuously optimized throughout various student projects supervised by the author [49–52]. Using this setup, several homogeneous animal tissues could be measured with an SPR accuracy of below 0.1% and compared to DECT and SECT predictions. The mean absolute prediction error was 0.2 % for DECT as compared to 1.5 % for SECT.

In the second and complementary project, an anthropomorphic head phantom was used to demonstrate the accuracy of DECT-based SPR prediction in a more realistic human morphology. Great care was taken to establish a proper virtual SPR ground truth for this phantom by reassigning SPR measured in separate homogeneous slabs to delineated material segmentations in a high-resolution CT scan of the phantom. This reference SPR map was also independently validated by comparing proton transmission measurements to Monte Carlo transport simulations based on the reference SPR map. In large homogeneous volumes of the phantom (brain, soft tissue, trabecular bone), DECT showed a median deviation to the reference below 1 % and thereby clearly outperformed SECT. In smaller volumes (cortical bone, sinus cavity) and at material edges, the comparison was inconclusive due to smoothing effects.

3.3 — Clinical relevance (IIIa-b)

Preceding the potential clinical implementation of the established approach for SPR prediction with DECT in ion treatment planning, it was tested on patient data. For this, a step-wise implementation was considered to gather initial clinical experience and DECT data for further investigation. In 2015 (2016), DECT was clinically implemented in proton (and photon) therapy by our collaboration partners at *OncoRay – National Center for Radiation Research in Oncology*, Dresden. As a conservative first step of clinical implementation, a look-up table is still applied, but to a pseudo-monoenergetic image derived from DECT (publication IIIa). In addition to potential advantages for diagnostic purposes and contouring due to the additional information in DECT images, a rapidly growing database of DECT images from more than 1400 patients as of November 2017 is available for research purposes.

This database could be used to compare the DECT-based SPR prediction with the current clinically used HLUT. Significant range differences of 1-4 mm (1-2 %) were found in 25 head and 25 prostate tumor patients, which are considered clinically relevant (publication IIIb).

Chapter 4

Publications

This thesis is presented in 'cumulative' format in accordance with the regulations of the Department of Physics and Astronomy of Heidelberg University. It comprises eight articles published in or submitted to internationally recognized peer-reviewed journals. The individual manuscripts are referred to within this thesis by roman numerals. Four manuscripts have been published (Ia, Ib, IIc, IIIa), two are accepted and 'in press' (IIb, IIIb) and another two are currently under review (Ic, IIa).

The dissertation is part of the joint funding project 'Translation of dual-energy CT into application in particle therapy' within the *National Center for Radiation Research in Oncology (NCRO)*. All work was performed in close collaboration with Patrick Wohlfahrt and Dr. Christian Richter from *OncoRay – National Center for Radiation Research in Oncology*, Dresden. The focus in Heidelberg was methodological and experimental development, while the clinical implementation and analysis of patient data was mainly performed in Dresden.

Accordingly, the author of this thesis is first author of publications Ia–IIa, shared first author of publication IIb and second author of publications IIc–IIIb. The specific authors' contributions to each article are stated in the respective following sections.

Ia — Methodological accuracy of image-based electron density assessment using dual-energy computed tomography

Authors: Christian Möhler, Patrick Wohlfahrt, Christian Richter, Steffen Greilich

Publication status (11/2017): Published

Journal reference: *Medical Physics*, vol. 44 (6), p. 2429, 2017

DOI: 10.1002/mp.12265

Authors' contributions: CM developed the presented theoretical framework and derived the results. PW verified the consistency of presented data and calculations. SG and CR supported integration of the study into the overall project strategy. CM drafted and revised the manuscript with critical review by all co-authors.

Ib — Range prediction for tissue mixtures based on dual-energy CT

Authors: Christian Möhler, Patrick Wohlfahrt, Christian Richter, Steffen Greilich

Publication status (11/2017): Published

Journal reference: *Physics in Medicine and Biology*, vol. 61 (11), p. N268, 2016

DOI: 10.1088/0031-9155/61/11/N268

Authors' contributions: CM conceived the presented approach and worked out the conceptual, mathematical and practical details in discussion with SG, PW and CR. PW verified the consistency of presented data and calculations. CM drafted and revised the manuscript with critical review by all co-authors.

Ic — On the common foundation of dual-energy CT methods for the determination of electron density and effective atomic number

Authors: Christian Möhler, Patrick Wohlfahrt, Christian Richter, Steffen Greilich

Publication status (11/2017): Under review in *Physics and Imaging in Radiation Oncology*

Authors' contributions: CM performed the presented theoretical work and calculations. PW independently verified the numerical results. CM drafted the manuscript with support from SG and critical review by PW and CR.

IIa — Experimental verification of particle-range prediction in biological tissue by single- and dual-energy computed tomography

Authors: Christian Möhler, Tom Russ, Patrick Wohlfahrt, Alina Elter, Armin Runz, Christian Richter, Steffen Greilich

Publication status (11/2017): Under review in *Physics in Medicine and Biology*

Preprint: arXiv:1708.07368

Authors' contributions: CM conceived the experimental study together with SG and was in charge of overall planning. CM, TR, AE, AR and SG developed and optimized the sample container and contributed to the final experimental design. AR prepared and performed 3D printing. TR and AR prepared the samples for measurement. CM, TR and AE carried out the experiments and performed data analysis. PW and CR supported integration of the study into the overall project strategy. CM drafted the manuscript with support from TR and critical review by SG, PW and CR.

IIb — Evaluation of stopping-power prediction by dual- and single-energy computed tomography in an anthropomorphic ground-truth phantom

Authors: Patrick Wohlfahrt[#], Christian Möhler[#], Christian Richter[**], Steffen Greilich[**]

[#] both authors share first authorship

[**] both authors share last authorship

Publication status (11/2017): In press, corrected proof

Journal reference: *International Journal of Radiation Oncology*Biology*Physics*, 2017

DOI: 10.1016/j.ijrobp.2017.09.025

Authors' contributions: All authors planned and conducted the proton-beam experiments. CR was in charge of overall coordination of the measurement campaign. PW performed the acquisition and processing of CT data. PW and CM analyzed the experimental data and prepared the results. SG designed, executed and evaluated the MC simulations. All authors discussed the results and shared in writing and revising the manuscript.

IIc — Comment on: Dosimetric comparison of stopping-power calibration with dual-energy CT and single-energy CT in proton therapy treatment planning [Med. Phys. 43(6), 2845-2854 (2016)]

Authors: Patrick Wohlfahrt, Christian Möhler, Steffen Greilich, Christian Richter

Publication status (11/2017): Published

Journal reference: *Medical Physics*, vol. 44 (10), p. 5533, 2017

DOI: 10.1002/mp.12418

Authors' contributions: PW and CM initially compiled the main points of criticism. PW and CR outlined the comment in consultation with CM and SG. PW performed all supportive calculations and drafted the manuscript with critical review by all co-authors.

IIIa — Clinical implementation of dual-energy CT for proton treatment planning on pseudo-monoenergetic CT scans

Authors: Patrick Wohlfahrt, Christian Möhler, Volker Hietschold, Stefan Menkel, Steffen Greilich, Mechthild Krause, Michael Baumann, Wolfgang Enghardt, Christian Richter

Publication status (11/2017): Published

Journal reference: *International Journal of Radiation Oncology*Biology*Physics*, vol. 97 (2), p. 427, 2017

DOI: 10.1016/j.ijrobp.2016.10.022

Authors' contributions: PW conceived the idea, designed and realized the basic clinical workflow and demonstrated its safe applicability in close collaboration with CR. VH (medical physicist in radiology), SM (medical physicist in proton therapy), MK, MB (clinical directors), WE (physics director) and CR (project leader) refined and approved the clinical implementation within their respective area of responsibility. PW performed the analysis and interpretation of image quality with support from CM. PW drafted and revised the manuscript with critical review by CR, CM and SG.

IIIb — Dual-energy CT based proton range prediction in head and pelvic tumor patients

Authors: Patrick Wohlfahrt, Christian Möhler, Kristin Stützer, Steffen Greilich, Christian Richter

Publication status (11/2017): In press, corrected proof

Journal reference: *Radiotherapy and Oncology*, 2017

DOI: 10.1016/j.radonc.2017.09.042

Authors' contributions: PW designed the study with support from CR and performed the evaluation of patient data. CM contributed to the implementation of the investigated approach. KS and PW conceptualized and supervised implementation of the employed raytracing algorithm. All authors intensively discussed the results and their role and implications for the overall project. PW drafted and revised the manuscript with critical review by all co-authors.

Chapter 5

Discussion

5.1 — Methodological development

5.1.1 Distinctive features

Aiming at optimal accuracy and clinical applicability, the established approach for DECT-based SPR prediction

A. is based on reconstructed images rather than projections,

B. factorizes into electron density and stopping number,

C. uses linear blending for electron density,

D. and uses cross section as a proxy for stopping number.

The individual features are discussed in the following subsections.

A. The algorithm is based on reconstructed images rather than projections

The determination of electron density and effective atomic number or, more generally, any processing of DECT data can be performed either in the projection or image domain, that is, during or after image reconstruction. Shortly after the invention of computed tomography, both the projection- and image-based algorithms were already prototyped by Alvarez & Macovski [22] and Brooks [24], respectively.

Algorithms operating on projection data allow to interact with image reconstruction and thereby, in principle, offer potential to reduce artifacts and noise. However, they might in turn require more assumptions and in particular a more specific parameterization of the photon attenuation cross section. Also, they might not be as easily calibrated [53]. But most importantly, projection-based algorithms require congruent beam projections and simultaneous acquisition of the projections for both spectra. This is not the case for many current clinical CT

scanners with dual energy (DE) functionality. Considering the goal of current clinical applicability, only image-based algorithms were included in the analysis [Ia-Ic].

Nevertheless, projection-based methods might become more interesting in the future with the advent of photon-counting CT detectors (see section 5.3.3). In these systems, only one x-ray tube is used while spectral separation is performed in the detector. The projections are thus always congruent in space and time.

B. Factorization into electron density and stopping number

DECT-based SPR prediction should be divided into the determination of electron density and stopping number for the following reasons:

- Both photons and ions, carrying an energy relevant to the discussed medical application, interact primarily with atomic electrons in the target. Consequently, electron density plays a fundamental role in both ion energy loss (SPR) and photon attenuation (CT number) and enters linearly in the according equations 2.4 and 2.6. Electron-density determination thus represents a 'natural' intermediate step in SPR prediction.
- We demonstrated that the determination of electron density from DECT data is simple, robust and has virtually negligible methodological uncertainty [Ia].
- Electron density dominates the variability in SPR of human tissue to about 95 % [Ib, section 2.2]. By its robust and accurate determination (see previous item), the largest part of the problem is already solved.
- By factorizing into electron density and stopping number, the empirical component (stopping number) is clearly isolated such that its impact on the overall uncertainty can be mitigated [Ib].
- Even if it is not explicitly calculated as part of an algorithm, electron-density information is always implicitly encoded simply due to the physics (see first item). For example, Taasti et al. [54] proposed a 2D empirical parameterization in dependence of the high- and low-energy CT numbers. However, the parameterization contains the exact term of linear blending that represents electron density [Ia]. As the primary advantage of their parameterization, Taasti et al. claim to reduce the number of required steps in the conversion from two to one. While this may be a correct observation from the methodological (or philosophical) point of view, it has no practical impact, as the equations for the two steps can equally be joined into one arithmetically.

C. Use linear blending for electron density

The rationale to use a simple linear-blending formula [Ia, equation 3] for DECT-based electron-density determination is elaborated in publication Ia from many different perspectives. The main line of argument is that with a methodological uncertainty of below 0.2 %, this method is already more than sufficiently accurate so that further complexity in the method is only counterproductive. More conceptual justifications for the linear-blending equation are [Ia, appendix]

i that it represents the only solution for electron density that is valid for any compound and not just single chemical elements and

ii that it follows as a mathematical implication from any definition of a single effective atomic number

D. Use cross section as a proxy for stopping number

Yang et al. [25] proposed an empirical relationship between the effective atomic number and the logarithm of the I-value, which can then be inserted into the Bethe formula (equation 2.5) to obtain stopping number and eventually SPR. From equations 2.4 and 2.6, it becomes clear that a more direct and intuitive way is to link the stopping number (instead of ln(I)) to the cross section (instead of effective atomic number).

In terms of image contrast, cross section and effective atomic number contain the same image information. Using an analogue from the field of image processing, the transformation between the two quantities can be viewed as a 'gamma correction' combined with a constant offset (cf., equation B7 in pub. Ib or equation 2 in pub. Ic). However, the use of cross sections ensures linear mixing and thus enables proper calibration (section 5.1.2) and quantification of uncertainty in the convex hull, as discussed in detail in publication Ib. The linear mixing property is conserved under any affine variable transformation such that a power of the effective atomic number, Z_{eff}^{m} with $m \approx 3$, might be used equivalently as a proxy for the stopping number.

5.1.2 Details of calibration

Choice of the cross section: To illustrate the general properties of the method, the lower-energy cross section, $\widehat{\sigma}_{\mathrm{l}}$, was initially chosen arbitrarily. In section 2.5 of publication Ib, it was already noted that any linear combination of $\widehat{\sigma}_{\mathrm{l}}$ and $\widehat{\sigma}_{\mathrm{h}}$ could be used preserving the linear mixing properties and all associated advantages. Such a linear combination corresponds to a pseudo-monoenergetic cross section. In the most recent publication, a monoenergetic cross section at 60 keV is

used [IIa]. One advantage of this is that the look-up table is completely independent of the CT scanner and protocol. A specific calibration of the cross section as described in section 2.4 of publication IIa is therefore obsolete. Furthermore, existing clinical software for DECT-based calculation of pseudo-monoenergetic images could be integrated into the workflow (see figure 3 in pub. IIa).

Choice of ion kinetic energy: A kinetic energy of 200 MeV/u was initially chosen [Ib] to calculate $\widehat{L}$ with equation 2.5, again with no consequence for the general conclusions derived. For application in patients, an effective energy of 100 MeV/u is recommended to minimize systematic bias due to the small energy dependence in SPR [55].

Shape of calibration curve: A very simple calibration line was originally defined to easily demonstrate the general mechanism of quantifying uncertainty in the convex hull. The calibration curve was later refined to better fit the most abundant human tissues in order to avoid systematic bias. The use of a piece-wise linear function conveniently suits the purpose and underlines the analogy to a HLUT (cf., figure 2 in pub. IIa).

Look-up table: A specific look-up table is provided in publication IIa (Table S3). Six reference human tissues or molecular base components from reference [48] are used as data points in the calibration. The selection of these is easier and less arbitrary than in the case of a HLUT, as their variance is reduced by definition (variance due to density is already removed).

Comment on the use of average bone tissues from White et al., 1987 [56]: For the calibration of a look-up table using human reference tissues, it is important to notice that the table for the elemental composition of human bones in White et al., 1987 [56, table V] lists large-scale volumetric averages (e.g., 'femur - spherical head', 'humerus - cylindrical shaft', see appendix A3). The tabulated data were accordingly intended for use in the manufacturing of radiological phantoms. However, they are of limited use for an analysis on smaller spatial scale (e.g., CT voxel). For the calibration of a look-up table, it is therefore crucial to include the base constituents of bones as documented in Woodard and White, 1986 [48], rather than the average bones. For example, trabecular bone is quite abundant in the pelvic region [IIIb] and should thus be considered in the calibration. Nevertheless, the average bones can be used to visualize the linear mixing behavior in the $\widehat{L}$ ($\widehat{\sigma}$)-plane as was done, for example, in figure 2 of publication IIa. These considerations apply in the same way to any definition of a look-up table, in particular the stoichiometric calibration.

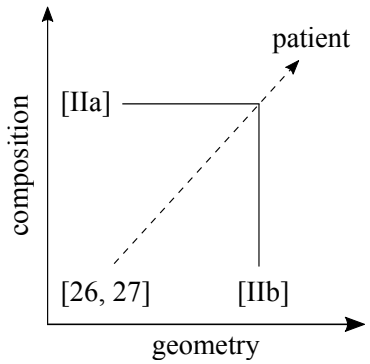

Figure 5: Schematic visualization of the overall strategy of experimental verification. One experiment was performed in each 'complexity dimension': animal tissues for composition [IIa] and the anthropomorphic head phantom for geometry [IIb]. Compared to a simple experiment using homogeneous tissue surrogates [26, 27], the 'extrapolation uncertainty' (visualized by the dashed lines) is reduced.

5.2 — Experimental verification

5.2.1 Overall strategy

Before the start of the NCRO project, experimental verification of DECT-based SPR prediction methods had been performed almost exclusively in homogeneous tissue surrogates, usually in the form of cylindrical inserts in a simple non-anthropomorphic phantom. Mean absolute deviations of DECT predictions in the order of 0.5 % had been observed [26, 27]. While an experiment of this type can serve as first test of a new method, the results should not be transferred to a patient case, due to the following main limitations:

i Composition: Tissue-surrogates are only approximately tissue equivalent, in particular for ion interaction, which is often not explicitly modeled. Since DECT-based SPR prediction still involves an empirical component, it should be tested in materials as similar to human tissue as possible. In an extreme case, a study that is purely based on non-tissue material can even lead to false conclusions, as demonstrated in publication IIc.

ii Geometry: Typical validation or calibration phantoms are also strongly simplified in geometry for practical reasons, ignoring heterogeneity, material transitions and all kinds of anisotropy.

In order to better approximate realistic composition and geometry, the pursued verification strategy was therefore to perform two experiments [IIa, IIb], in which one parameter each was kept simple, while the other was made as realistic as possible. The combined results are then projected to the patient case with reduced 'extrapolation uncertainty' (figure 5).

5.2.2 Experimental uncertainty of SPR reference

The goal of the experiments was to allow evaluation of absolute SPR prediction at an uncertainty level of below 1 % (cf., section 1.2) and thus to enable discrimination between the performance of different methods, in particular DECT vs. SECT. Therefore, a major part of the experimental development was dedicated to minimizing experimental uncertainty. For the anthropomorphic head phantom, a full virtual 3D reference map was established with a validated uncertainty in SPR and range within 0.3 % and 1 mm, respectively [IIb].

The experimental setup described and used in publication IIa for the measurement of animal tissues, was developed and optimized in the course of four student projects [49–52]. Compared to previous experiments of similar type [15, 57, 58], a substantial increase in accuracy was achieved by design of the 3D-printed sample container, which is carefully adapted to match the specific requirements of both the DECT scanner and the ion beam line [IIa, figure 1]. The uncertainty component due to sample thickness is thus eliminated, which reduces experimental uncertainty for a homogeneous substance (ideally liquid) to below 0.1 %. At this uncertainty level, the developed experimental setup can also be used for the determination of I-values (section 5.4.2).

5.2.3 Accuracy of SPR prediction

In both experimental settings, DECT showed considerably superior accuracy in SPR prediction compared to the standard HLUT-based approach (see summary of results in section 3). According to the overall strategy of experimental verification (figure 5), a similar advantage of DECT in SPR accuracy can thus be expected in clinical setting.

5.3 — CLINICAL RELEVANCE

5.3.1 Impact on range uncertainty

The impact of SPR uncertainty on dose or ion-range uncertainty is rather non-trivial and case-dependent. For the evaluated example treatment plan in the head phantom, significant difference in ion ranges were not observed between the different evaluated methods, despite considerable differences in the performance on voxel-wise SPR level. This is due to a partly dominating, additional effect that was observed at material transitions, which lead to compensation of systematic SPR prediction error in some cases [IIb, figure 5].

On the other hand, the relative comparison in a patient cohort showed signifi-

cant range differences of clinical relevance between the DECT- and HLUT-based methods [IIIb]. Here, data suggests that a systematic mean (or median) SPR bias in the irradiated volume translates into a mean (or median) range bias of roughly the same magnitude [IIIb, figure 4], which can be also intuitively expected. This indicates that a net advantage in SPR prediction might directly translate into an net advantage in range prediction.

5.3.2 Practical considerations for clinical implementation

For the publications IIa, IIb and IIIb, a mix of existing clinical software (mainly Siemens syngo.CT DE Rho/Z and Monoenergetic Plus) and self-written Python scripts was used. The specific implementations are described in the respective papers (e.g., figure 3 in pub. IIa). For the clinical use outside a defined research environment, however, it will be necessary to implement the full chain in certified medical products. This could be done either in the post-processing software that is provided with CT scanners or inside the treatment planning system (TPS). The following scenarios are therefore possible:

A complete implementation in CT software (interface SPR)

B complete implementation in TPS (interface CT number)

C shared implementation (interface, e.g., electron density/cross section)

Version A might be preferable to decrease image noise and artifacts in the final SPR image. Algorithms for this purpose are already implemented, for example, in the above-mentioned clinical software applications and they could be directly transferred to the calculation of SPR.

5.3.3 Future technological development

Currently, a new generation of CT detectors is being developed. Replacing the rather slow scintillating crystal of conventional energy-integrating detectors by a semi-conductor with fast read-out electronics, the registration of single photons is possible [59]. By setting different thresholds on the signal, incoming photons can be sorted into multiple energy bins, enabling spectral applications [60].

One advantage of the so-called photon-counting CT is the automatic availability of spectral information with every scan without specific settings so that multi-energy functionality can naturally find broader application. Furthermore, the system could remove certain limitations of current DECT technology, such as the small field of view of current dual-source systems or the time offset between the two projections in the sequential scanning technique.

5.4 — ADDITIONAL APPLICATIONS OF DUAL-ENERGY CT IN RADIATION THERAPY

Alongside the main focus of this thesis, as reflected in the publications, further potential applications of DECT in radiation therapy were investigated, mainly in associated student projects supervised by the author [49–52, 61].

5.4.1 Dual-energy CT for non-tissue material

The benefit of DECT can be particularly large in the presence of non-tissue materials such as implants or contrast agent, which are generally not well represented by a HLUT (section 2.3.3). The applications, described in the next two paragraphs, are expected to be of potential relevance for conventional photon therapy in addition to ion therapy. For dose calculation in photon therapy, the quantity of interest is electron density instead of SPR.

Identification and quantification of implants

Many radiotherapy patients have implants, which usually need to be contoured and overridden in the CT image during treatment planning. A practical problem is the often unknown composition of the implant, which makes the correct assignment of electron density and SPR difficult[1]. DECT could help in both characterizing the implant and calculate a more accurate electron density and SPR (within potential limitation at higher atomic numbers [Ia] or due to the remaining empirical component [Ib]). The extra step of contouring might even become obsolete. First experiments with PALACOS® bone cement (Heraeus Medical) and interbody fusion cages (type 'Harms') are documented in a master's thesis [61]. The results underline the potential of DECT to better quantify electron density and SPR of the investigated materials.

Dose calculation on DECT scans with iodinated contrast agent

An iodinated contrast agent is commonly used in pre-treatment imaging to support tumor diagnostics and delineation. A second 'native' CT scan (i.e., without contrast medium), is then required for dose calculation, as the large atomic number of iodine hampers CT conversion via an HLUT. On the other hand, electron density should remain almost unaffected by the contrast agent due to its low concentration in tissue. An electron-density image derived from contrast-enhanced DECT should therefore resemble a native electron-density image. Dose calculation based on a DECT scan with contrast agent is therefore conceivable. The

[1] Personal communication, B. Ackermann, Heidelberg Ion Beam Therapy Center (HIT)

additional native scan would become obsolete, leading to a simplified workflow and a reduction of the patient dose by half.

The remaining impact of contrast agent on DECT-derived electron-density and SPR images was studied in a dilution series of Imeron® 300 (Bracco Imaging Deutschland GmbH, Germany) over a range of typical iodine concentrations [61]. The impact on both electron density and SPR could be limited to 1 % instead of 5-10 % when using contrast-enhanced single-energy computed tomography (SECT).

A clinical trial is currently underway at DKFZ to investigate patient treatment planning based on contrast-enhanced DECT.

5.4.2 Measurement of I-values

The developed experimental setup [IIa] can be used for the measurement of I-values. For this application, DECT serves as an efficient tool to eliminate electron density (equation 2.4). Due to the logarithmic dependence of the stopping number on the I-value (equation 2.3), the achieved reduction of uncertainty in the measurement of both SPR and electron density is essential here. Besides, the setup was optimized for high sample throughput, for example, by using a remote-controlled linear table. With a rate of below two minutes per sample, it is possible to acquire sufficient statistics to quantify uncertainty or variability.

In this way, the method was applied in one of the above-mentioned projects to determine elemental I-values by multivariate regression to measurements of aqueous solutions [51]. The I-value of phosphorus was found to be significantly lower than the literature value, which would have an impact on any calibrated SPR prediction for bone.

Further experiments of the described type can be performed in the future, for example, to investigate natural I-value variability in tissue or to determine the I-value of water, which is of immediate relevance to ion therapy and still subject to considerable uncertainty [62, 63].

Chapter 6

Summary

An optimized approach for stopping-power ratio (SPR) prediction with clinical dual-energy computed tomography (DECT) was established, experimentally validated and clinically tested.

The refinement of algorithms based on reconstructed images rather than projections allowed for immediate application using common DECT technology, where the high- and low-energy projections are often not congruent in space or time. The 'natural' decomposition into separate determination of electron density and stopping number (i.e., the two basic dependencies in SPR) minimized the impact of the empirical component. This in turn maximizes the methodological benefits of using DECT compared to SECT, since the limitations of a SECT-based HLUT approach (ambiguous, static, not patient specific) can be ascribed mainly to its empirical nature.

In the first step of the developed approach, electron density was obtained from DECT data by a simple one-parametric linear-blending formula. The methodological uncertainty was shown to be below 0.2 % for arbitrary mixtures of human tissue and for any calibrated DECT system. A simple method for the calibration of the linear-blending parameter was proposed. The approach was also conceptually justified as the only universal solution that is valid for both pure elements and chemical compounds.

To obtain the stopping number in the second step, we proposed to use the photon absorption cross section obtained from DECT as an empirical proxy rather than the effective atomic number. This ensures, among other advantages, a proper treatment of mixtures, which are crucial in CT imaging on all scales from microscopic to voxel level. This linear mixing property enables simple and effective calibration using a piecewise linear function in analogy to an HLUT. Furthermore, an upper limit of uncertainty of 0.6 % was determined for arbitrary mixtures of human tissues from their convex hull in the $(\widehat{\sigma}, \widehat{L})$ variable space.

Comprehensive experimental verification of the established approach was performed to investigate its accuracy in a scenario of advanced complexity in either

composition (animal tissues) or geometric morphology (anthropomorphic phantom). By keeping the other aspect simplified in each case, an SPR reference was established with an uncertainty of 0.1 % and 0.3 %, respectively. This enabled sub-percent discrimination of the performance of different methods. In animal tissues, a mean absolute prediction error of 0.2 % was found for DECT as compared to 1.5 % for SECT. In the main components of the anthropomorphic head phantom (brain, soft tissue, trabecular bone), the median deviation to the reference was less than 1 %. In both scenarios, DECT-based SPR prediction thus demonstrated superior accuracy compared to the standard clinical HLUT-based method.

A relative comparison in 50 head and prostate tumor patients from a database of clinical DECT scans revealed significant mean range differences of about 1 mm (head) and 4 mm (prostate) between the optimized approach and the clinical standard, thus highlighting clinical relevance. The established method can be readily implemented either by the CT vendor or in the treatment planning system. Additional applications of DECT in both photon and ion radiation therapy are conceivable with a more practical benefit such as the simplification of treatment planning workflow and reduction of patient dose by performing dose calculation on contrast-enhanced DECT scans.

In conclusion, a reduction of the uncertainty in SPR prediction to below 1 % was demonstrated using currently available DECT imaging technology. The benefit in voxelwise SPR prediction most probably translates to an advantage of similar magnitude in ion ranges. Whether this may ultimately lead to a reduction of treatment margins remains to be investigated by taking other sources of range uncertainty into account.

Appendix

A1 — Corrections to the Bethe formula

In its quantum mechanical derivation, the stopping number, L, is expanded in a perturbation series in z such that

$$L(\beta) = L_0 + zL_1 + z^2 L_2 \,. \tag{A.1}$$

The higher-order Barkas and Bloch terms, zL_1 and z^2L_2 respectively, are important only at low projectile energy. The leading term

$$L_0 = \frac{1}{2} \ln \left(\frac{2m_\mathrm{e}c^2\beta^2 W_\mathrm{m}}{1-\beta^2} \right) - \beta^2 - \ln I - C/Z - \delta/2 \tag{A.2}$$

depends on the maximum energy transfer to a free electron in one collision, W_m, and on the mean excitation energy or 'I-value', I, of the medium. The shell correction, $-C/Z$, becomes relevant at low energy, when the velocity of target electrons cannot be neglected compared to the projectile velocity. The density correction, $-\delta/2$, accounts for the polarization of the target medium at high energy. Both corrections can be neglected in the intermediate energy regime relevant to ion therapy. For heavy charged particles of mass M with $m_\mathrm{e}/M \ll 1$ (protons, alphas, ions), W_m, can be written

$$W_\mathrm{m} = \frac{2m_\mathrm{e}c^2\beta^2}{1-\beta^2} \cdot \left[1 + 2\frac{m_\mathrm{e}/M}{(1-\beta^2)^{1/2}} + (m_\mathrm{e}/M)^2 \right]^{-1} . \tag{A.3}$$

The factor in square brackets deviates from unity only about 0.1 % (0.01 %) for proton (carbon ions) at 100 MeV/u. Setting it to unity cancels the dependence on the projectile mass and simplifies equation A.2, leading to

$$L \approx \ln \left(\frac{2m_\mathrm{e}c^2\beta^2}{1-\beta^2} \right) - \beta^2 - \ln I \,, \tag{A.4}$$

which corresponds to equation 2.3.

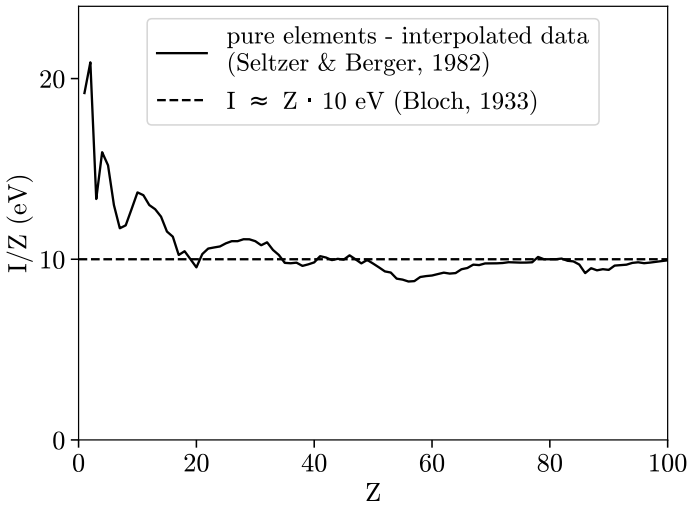

Figure 6: Relation between I-value, I, and atomic number, Z.

A2 — Mean excitation energies (I-values)

For pure elements, I-values show a rough correlation with the atomic number, Z, [64]

$$I \approx Z \cdot 10\,\mathrm{eV}\,, \tag{A.5}$$

which applies mainly to higher atomic numbers of about $Z > 20$ (figure 6).

The data source for elemental I-values used in this thesis is the compilation by Seltzer & Berger, 1982 [65]. Apart from a list of I-values of pure elements [65, table 2], they also included recommendations [65, table 6] for adapted elemental I-values to be used in the calculation of compound I-values via Bragg's additivity rule [66].

A3 — The composition of body tissues

Due to the (at least partly) empirical nature of CT-based SPR prediction, certain knowledge on the elemental composition of tissues is essential. An exhaustive compilation of data available today was performed by Woodard & White, 1986 [48]. For their article entitled 'The composition of body tissues', they collected and reprocessed data from several older studies including the compilation in the 'Report of the task group on reference man' by the International Commission on Radiological Protection (ICRP) from 1975 [67]. The tabulated data in reference [48] comprises 56 tissues, including the five base constituents of bones: cortical bone, red marrow, yellow marrow, spongiosa and cartilage. For seven tis-

sues (e.g., adipose and muscle), the data quality was sufficient to infer the spread in composition in addition to a single value or population mean.

One year later in 1987, White et al. published 'average soft-tissue and bone models for use in radiation dosimetry' [56], based on volumetric averages of the previously listed individual tissues according to simple geometrical models of specific body regions. Concerning the average bones, the provided data are an update of a previous publication [68], using the more recent values for the bone base constituents from reference [48].

All mentioned sources refer to healthy adults, apart from a table on the age-dependent variation of calcium content in cortical bone [48, table IV]. In 1991, the data on tissue composition was therefore complemented by analyzing various age groups 'from fetus to young adult' [69].

The most current reports from the International Commission on Radiation Units and Measurements (ICRU) mentioning tissue composition in a given context, for example, the reports 44, 46 and 73 [70–72], as well as ICRP report 89 [73] mostly reproduce the tables of the above-described publications by Woodard, White et al. [48, 56, 69]. To the best knowledge of the author, these tables still represent the most encompassing compilation. It is therefore recommended to use these tables directly, rather than the derivatives in the ICRU reports or in Schneider et al., 2000 [74].

Bibliography

[1] Baumann M, Krause M, Overgaard J, Debus J, Bentzen SM, Daartz J, et al. Radiation oncology in the era of precision medicine. Nature Reviews Cancer. 2016;16(4):234–249. doi:10.1038/nrc.2016.18.

[2] Wilson RR. Radiological Use of Fast Protons. Radiology. 1946;47(5):487–491. doi:10.1148/47.5.487.

[3] Böhlen TT, Cerutti F, Chin MPW, Fassò A, Ferrari A, Ortega PG, et al. The FLUKA Code: Developments and Challenges for High Energy and Medical Applications. Nuclear Data Sheets. 2014;120:211–214. doi:10.1016/j.nds.2014.07.049.

[4] Ferrari A, Sala PR, Fasso A, Ranft J. FLUKA: A Multi-Particle Transport Code. Menlo Park, CA: Stanford Linear Accelerator Center (SLAC); 2005. doi:10.2172/877507.

[5] Paganetti H. Range uncertainties in proton therapy and the role of Monte Carlo simulations. Physics in Medicine and Biology. 2012;57(11):R99–R117. doi:10.1088/0031-9155/57/11/R99.

[6] Knopf AC, Lomax A. In vivo proton range verification: a review. Physics in Medicine and Biology. 2013;58(15):R131–60. doi:10.1088/0031-9155/58/15/R131.

[7] Bert C, Durante M. Motion in radiotherapy: particle therapy. Physics in Medicine and Biology. 2011;56(16):R113–R144. doi:10.1088/0031-9155/56/16/R01.

[8] Knopf AC, Stützer K, Richter C, Rucinski A, da Silva J, Phillips J, et al. Required transition from research to clinical application: Report on the 4D treatment planning workshops 2014 and 2015. Physica Medica. 2016;32(7):874–882. doi:10.1016/j.ejmp.2016.05.064.

[9] Li H, Zhang X, Park P, Liu W, Chang J, Liao Z, et al. Robust optimization in intensity-modulated proton therapy to account for anatomy changes in lung cancer patients. Radiotherapy and Oncology. 2015;114(3):367–372. doi:10.1016/j.radonc.2015.01.017.

[10] van der Voort S, van de Water S, Perkó Z, Heijmen B, Lathouwers D, Hoogeman M. Robustness Recipes for Minimax Robust Optimization in Intensity Modulated Proton Therapy for Oropharyngeal Cancer Patients. International Journal of Radiation Oncology*Biology*Physics. 2016;95(1):163–170. doi:10.1016/j.ijrobp.2016.02.035.

[11] Barker JL, Garden AS, Ang KK, O'Daniel JC, Wang H, Court LE, et al. Quantification of volumetric and geometric changes occurring during fractionated radiotherapy for head-and-neck cancer using an integrated CT/linear accelerator system. International Journal of Radiation Oncology*Biology*Physics. 2004;59(4):960–970. doi:10.1016/j.ijrobp.2003.12.024.

[12] Stützer K, Jakobi A, Bandurska-Luque A, Barczyk S, Arnsmeyer C, Löck S, et al. Potential proton and photon dose degradation in advanced head and neck cancer patients by intratherapy changes. Journal of Applied Clinical Medical Physics. 2017;18(6):104–113. doi:10.1002/acm2.12189.

[13] ICRU. Report 78: Prescribing, Recording, and Reporting Proton-Beam Therapy. Journal of the ICRU. 2007;7(2). doi:10.1093/jicru/ndn001.

[14] Goitein M. Calculation of the uncertainty in the dose delivered during radiation therapy. Medical Physics. 1985;12(5):608–612. doi:10.1118/1.595762.

[15] Schaffner B, Pedroni E. The precision of proton range calculations in proton radiotherapy treatment planning: experimental verification of the relation between CT-HU and proton stopping power. Physics in Medicine and Biology. 1998;43(6):1579–1592. doi:10.1088/0031-9155/43/6/016.

[16] Moyers MF, Miller DW, Bush DA, Slater JD. Methodologies and tools for proton beam design for lung tumors. International Journal of Radiation Oncology*Biology*Physics. 2001;49(5):1429–1438. doi:10.1016/S0360-3016(00)01555-8.

[17] Yang M, Zhu XR, Park PC, Titt U, Mohan R, Virshup G, et al. Comprehensive analysis of proton range uncertainties related to patient stopping-power-ratio estimation using the stoichiometric calibration. Physics in Medicine and Biology. 2012;57(13):4095–4115. doi:10.1088/0031-9155/57/13/4095.

[18] Penfold SN, Rosenfeld AB, Schulte RW, Schubert KE. A more accurate reconstruction system matrix for quantitative proton computed tomography. Medical Physics. 2009;36(10):4511–4518. doi:10.1118/1.3218759.

[19] Poludniowski G, Allinson NM, Evans PM. Proton radiography and tomography with application to proton therapy. The British Journal of Radiology. 2015;88(1053):20150134. doi:10.1259/bjr.20150134.

[20] Johnson RP, Bashkirov V, DeWitt L, Giacometti V, Hurley RF, Piersimoni P, et al. A Fast Experimental Scanner for Proton CT: Technical Performance and First Experience With Phantom Scans. IEEE Transactions on Nuclear Science. 2016;63(1):52–60. doi:10.1109/TNS.2015.2491918.

[21] Flohr TG, McCollough CH, Bruder H, Petersilka M, Gruber K, Christoph S, et al. First performance evaluation of a dual-source CT (DSCT) system. European Radiology. 2006;16(2):256–268. doi:10.1007/s00330-005-2919-2.

[22] Alvarez RE, Macovski A. Energy-selective reconstructions in X-ray computerised tomography. Physics in Medicine and Biology. 1976;21(5):002. doi:10.1088/0031-9155/21/5/002.

[23] Rutherford RA, Pullan BR, Isherwood I. Measurement of effective atomic number and electron density using an EMI scanner. Neuroradiology. 1976;11(1):15–21. doi:10.1007/BF00327253.

[24] Brooks RA. A Quantitative Theory of the Hounsfield Unit and Its Application to Dual Energy Scanning. Journal of Computer Assisted Tomography. 1977;1(4):487–493. doi:10.1097/00004728-197710000-00016.

[25] Yang M, Virshup G, Clayton J, Zhu XR, Mohan R, Dong L. Theoretical variance analysis of single- and dual-energy computed tomography methods for calculating proton stopping power ratios of biological tissues. Physics in Medicine and Biology. 2010;55(5):1343–1362. doi:10.1088/0031-9155/55/5/006.

[26] Hünemohr N, Krauss B, Tremmel C, Ackermann B, Jäkel O, Greilich S. Experimental verification of ion stopping power prediction from dual energy CT data in tissue surrogates. Physics in Medicine and Biology. 2014;59(1):83–96. doi:10.1088/0031-9155/59/1/83.

[27] Bourque AE, Carrier JF, Bouchard H. A stoichiometric calibration method for dual energy computed tomography. Physics in Medicine and Biology. 2014;59(8):2059–88. doi:10.1088/0031-9155/59/8/2059.

[28] Heismann BJ, Leppert J, Stierstorfer K. Density and atomic number measurements with spectral x-ray attenuation method. Journal of Applied Physics. 2003;94(3):2073–2079. doi:10.1063/1.1586963.

[29] Bazalova M, Carrier JF, Beaulieu L, Verhaegen F. Dual-energy CT-based material extraction for tissue segmentation in Monte Carlo dose calculations. Physics in Medicine and Biology. 2008;53(9):2439–2456. doi:10.1088/0031-9155/53/9/015.

[30] Saito M. Potential of dual-energy subtraction for converting CT numbers to electron density based on a single linear relationship. Medical Physics. 2012;39(4):2021. doi:10.1118/1.3694111.

[31] Landry G, Seco J, Gaudreault M, Verhaegen F. Deriving effective atomic numbers from DECT based on a parameterization of the ratio of high and low linear attenuation coefficients. Physics in Medicine and Biology. 2013;58(19):6851–6866. doi:10.1088/0031-9155/58/19/6851.

[32] van Abbema JK, van Goethem MJ, Greuter MJW, van der Schaaf A, Brandenburg S, van der Graaf ER. Relative electron density determination using a physics based parameterization of photon interactions in medical DECT. Physics in Medicine and Biology. 2015;60(9):3825. doi:10.1088/0031-9155/60/9/3825.

[33] Garcia LIR, Azorin JFP, Almansa JF. A new method to measure electron density and effective atomic number using dual-energy CT images. Physics in Medicine and Biology. 2016;61(1):265–279. doi:10.1088/0031-9155/61/1/265.

[34] Saito M, Sagara S. A simple formulation for deriving effective atomic numbers via electron density calibration from dual-energy CT data in the human body. Medical Physics. 2017;44(6):2293–2303. doi:10.1002/mp.12176.

[35] Bethe H. Zur Theorie des Durchgangs schneller Korpuskularstrahlen durch Materie. Annalen der Physik. 1930;397(3):325–400. doi:10.1002/andp.19303970303.

[36] Berger MJ, Coursey JS, Zucker MA, Chang J. ESTAR, PSTAR, and ASTAR: Computer Programs for Calculating Stopping-Power and Range Tables for Electrons, Protons, and Helium Ions (version 2.0.1). Available: http://physics.nist.gov/Star [nov 2017]. National Institute of Standards and Technology, Gaithersburg, MD; 2017.

[37] Jackson DF, Hawkes DJ. X-ray attenuation coefficients of elements and mixtures. Physics Reports. 1981;70(3):169–233. doi:10.1016/0370-1573(81)90014-4.

[38] Berger M, Hubbell J, Seltzer S, Chang J, Coursey J, Sukumar R, et al.. XCOM: Photon Cross Section Database (version 1.5). Available: http://physics.nist.gov/xcom [nov 2017]. National Institute of Standards and Technology, Gaithersburg, MD; 2010.

[39] Hounsfield GN. Computerized transverse axial scanning (tomography): Part 1. Description of system. The British Journal of Radiology. 1973;46(552):1016–1022. doi:10.1259/0007-1285-46-552-1016.

[40] Macovski A, Alvarez R, Chan JLH, Stonestrom JP, Zatz LM. Energy dependent reconstruction in X-ray computerized tomography. Computers in Biology and Medicine. 1976;6(4):325–336. doi:10.1016/0010-4825(76)90069-X.

[41] Lehmann LA, Alvarez RE, Macovski A, Brody WR, Pelc NJ, Riederer SJ, et al. Generalized image combinations in dual KVP digital radiography. Medical Physics. 1981;8(5):659–667. doi:10.1118/1.595025.

[42] Petersilka M, Bruder H, Krauss B, Stierstorfer K, Flohr TG. Technical principles of dual source CT. European Journal of Radiology. 2008;68(3):362–368. doi:10.1016/j.ejrad.2008.08.013.

[43] Leschka S, Stolzmann P, Schmid FT, Scheffel H, Stinn B, Marincek B, et al. Low kilovoltage cardiac dual-source CT: attenuation, noise, and radiation dose. European Radiology. 2008;18(9):1809–1817. doi:10.1007/s00330-008-0966-1.

[44] Saba L, Porcu M, Schmidt B, Flohr T. Dual Energy CT: Basic Principles. In: Dual Energy CT in Oncology. Cham: Springer International Publishing; 2015. p. 1–20. doi:10.1007/978-3-319-19563-6_1.

[45] Almeida IP, Schyns LEJR, Öllers MC, van Elmpt W, Parodi K, Landry G, et al. Dual-energy CT quantitative imaging: a comparison study between twin-beam and dual-source CT scanners. Medical Physics. 2017;44(1):171–179. doi:10.1002/mp.12000.

[46] Jäkel O, Jacob C, Schardt D, Karger CP, Hartmann GH. Relation between carbon ion ranges and x-ray CT numbers. Medical physics. 2001;28(4):701–703. doi:10.1118/1.1357455.

[47] Schneider U, Pedroni E, Lomax A. The calibration of CT Hounsfield units for radiotherapy treatment planning. Physics in Medicine and Biology. 1996;41(1):111–124. doi:10.1088/0031-9155/41/1/009.

[48] Woodard HQ, White DR. The composition of body tissues. The British Journal of Radiology. 1986;59(708):1209–1218. doi:10.1259/0007-1285-59-708-1209.

[49] Russ T. Dual-energy CT and ion range measurement of animal tissue for application in ion radiotherapy [Bachelor thesis]. Heidelberg University; 2016.

[50] Elter A. Dual-energy CT and ion range measurements of tissue base components for application in radiotherapy [Bachelor thesis]. Heidelberg University; 2016.

[51] Latz B. Determination of I-values Relevant to Radiotherapy Measuring X-ray and Ion Interaction in Aqueous Solutions [Bachelor thesis]. Heidelberg University; 2016.

[52] Russ T. (soon to be submitted) [Master thesis]. Heidelberg University; 2017.

[53] Tremblay J, Bedwani S, Bouchard H. A theoretical comparison of tissue parameter extraction methods for dual energy computed tomography. Medical Physics. 2014;41(8Part1):081905. doi:10.1118/1.4886055.

[54] Taasti VT, Petersen JBB, Muren LP, Thygesen J, Hansen DC. A robust empirical parametrization of proton stopping power using dual energy CT. Medical Physics. 2016;43(10):5547–5560. doi:10.1118/1.4962934.

[55] Inaniwa T, Kanematsu N. Effective particle energies for stopping power calculation in radiotherapy treatment planning with protons and helium, carbon, and oxygen ions. Physics in Medicine and Biology. 2016;61(20):N542–N550. doi:10.1088/0031-9155/61/20/N542.

[56] White DR, Woodard HQ, Hammond SM. Average soft-tissue and bone models for use in radiation dosimetry. The British Journal of Radiology. 1987;60(717):907–913. doi:10.1259/0007-1285-60-717-907.

[57] Rietzel E, Schardt D, Haberer T. Range accuracy in carbon ion treatment planning based on CT-calibration with real tissue samples. Radiation Oncology. 2007;2(1):14. doi:10.1186/1748-717X-2-14.

[58] Zhang R, Baer E, Jee KW, Sharp G, Lu HM. Investigation of real tissue water equivalent path lengths using an efficient dose extinction method. Physics in Medicine and Biology. 2017;62:5640–5651. doi:10.1088/1361-6560/aa782c.

[59] Taguchi K, Iwanczyk JS. Vision 20/20: Single photon counting x-ray detectors in medical imaging. Medical Physics. 2013;40(10):100901. doi:10.1118/1.4820371.

[60] Leng S, Zhou W, Yu Z, Halaweish A, Krauss B, Schmidt B, et al. Spectral performance of a whole-body research photon counting detector CT: quantitative accuracy in derived image sets. Physics in Medicine and Biology. 2017;62(17):7216–7232. doi:10.1088/1361-6560/aa8103.

[61] Böswald V. Zweispektren-Computertomographie für die Photonen- und Ionentherapiepla-

nung [Master thesis]. Eberhard Karls Universität Tübingen; 2016.

[62] Andreo P. On the clinical spatial resolution achievable with protons and heavier charged particle radiotherapy beams. Physics in Medicine and Biology. 2009;54(11):N205–N215. doi:10.1088/0031-9155/54/11/N01.

[63] ICRU. Report 90: Key data for ionizing-radiation dosimetry: measurement standards and applications. Journal of the ICRU. 2014;14(1):3–4. doi:10.1093/jicru/ndw029.

[64] Bloch F. Zur Bremsung rasch bewegter Teilchen beim Durchgang durch Materie. Annalen der Physik. 1933;408(3):285–320. doi:10.1002/andp.19334080303.

[65] Seltzer SM, Berger MJ. Evaluation of the collision stopping power of elements and compounds for electrons and positrons. The International Journal of Applied Radiation and Isotopes. 1982;33(11):1189–1218. doi:10.1016/0020-708X(82)90244-7.

[66] Bragg WH, Kleeman R. XXXIX. On the α particles of radium, and their loss of range in passing through various atoms and molecules. Philosophical Magazine Series 6. 1905;10(57):318–340. doi:10.1080/14786440509463378.

[67] ICRP. Report 23: Report of the task group on Reference Man. Oxford: International commission on radiological protection; 1975.

[68] Woodard HQ, White DR. Bone models for use in radiotherapy dosimetry. The British Journal of Radiology. 1982;55(652):277–282. doi:10.1259/0007-1285-55-652-277.

[69] White DR, Widdowson EM, Woodard HQ, Dickerson JWT. The composition of body tissues. (II) Fetus to young adult. The British Journal of Radiology. 1991;64(758):149–159. doi:10.1259/0007-1285-64-758-149.

[70] ICRU. Report 44: Tissue substitutes in radiation dosimetry and measurement. International commission on radiation units and measurements; 1989.

[71] ICRU. Report 46: Photon, electron, proton and neutron interaction data for body tissues. International commission on radiation units and measurements; 1992.

[72] ICRU. Report 73: Stopping of ions heavier than helium. International commission on radiation units and measurements; 2005. doi:10.1093/jicru/ndi001.

[73] ICRP. Report 89: Basic anatomical and physiological data for use in radiological protection: reference values; 2002.

[74] Schneider W, Bortfeld T, Schlegel W. Correlation between CT numbers and tissue parameters needed for Monte Carlo simulations of clinical dose distributions. Physics in Medicine and Biology. 2000;45(2):459–478. doi:10.1088/0031-9155/45/2/314.

Acknowledgments

First of all, I wish to thank Prof. Dr. Oliver Jäkel for the opportunity to pursue this project in the *Division of Medical Physics in Radiation Oncology* at DKFZ. I thank him and Prof. Dr. João Seco for agreeing to act as referees for this thesis.
I am deeply grateful to my supervisor Dr. Steffen Greilich for his outstanding support. Besides his multifaceted and continuous advice, I greatly appreciate his inspiring knowledge and open-mindedness.
The success of this project was immensely promoted by collaboration with our NCRO research partners. I therefore owe a very special thank to Dr. Christian Richter and Patrick Wohlfahrt for the exceptional team work and many inspiring meetings in Dresden and Heidelberg.
I would like to thank Prof. Dr. Oliver Jäkel, Prof. Dr. Marc Kachelrieß, Dr. Christian Richter and Dr. Steffen Greilich for their guidance as members of my 'Thesis Advisory Committee'.
I would also like to express my gratitude to Tom Russ, Alina Elter, Beatrice Latz and Verena Böswald for their valuable contributions to the DECT project in the course of their respective thesis projects in our group.
Prof. Dr. Heinz-Peter Schlemmer and the radiology department are acknowledged for granting us access to the dual-energy CT scanner at DKFZ. Many thanks to the Heidelberg Ion Beam Therapy Center (HIT) for providing beam time for our experimental projects.
I am thankful to everyone who supported our experiments and studies, in particular Armin Runz and the workshop, Dr. Stephan Brons and Martina Jochim.
I wish to thank PD Dr. Nils Nicolay, PD Dr. Henrik Hauswald and Prof. Dr. Florian Sterzing from the clinical cooperation unit, as well as Dr. Peter Häring, Clemens Lang and Mona Splinter for collaboration in the patient-related projects.
I also wish to thank Benjamin Ackermann and Dr. Malte Ellerbrock for enhancing the DECT discussion from the perspective of clinical medical physicists.
Finally, I am grateful to all my colleagues from the working group and department for the very pleasant atmosphere at work.
The National Center for Radiation Research in Oncology (NCRO) is acknowledged for providing funding for this dissertation within the project 'Translation of dual-energy CT into application in particle therapy'.